Springer Proceedings in Mathematics & Statistics

Christian Klingenberg
Michael Westdickenberg *Editors*

Theory, Numerics and Applications of Hyperbolic Problems I

Aachen, Germany, August 2016

Springer

Well-Balanced Central-Upwind Schemes for 2 × 2 Systems of Balance Laws

Alina Chertock, Michael Herty and Şeyma Nur Özcan

Abstract In this study, we have developed a well-balanced second-order central-upwind scheme for 2×2 systems of balance laws, in particular, the models of isothermal gas dynamics with source and traffic flow with relaxation to equilibrium velocities. The new scheme is based on modifications in the reconstruction and evolution steps of a Godunov-type central-upwind method. The first step of this modification is to introduce an equilibrium variable obtained from incorporating the source term into the flux. By reconstructing equilibrium variables and using them in the well-balanced evolution process, we have illustrated that the proposed scheme being well balanced, namely, it preserves steady states of the system.

Keywords Well-balanced schemes · 2×2 system of balance laws

1 Introduction

We consider a 2×2 system of equations of the following type:

$$\begin{cases} \rho_t + f_1(\rho, q)_x = 0, \\ q_t + f_2(\rho, q)_x = -s(\rho, q), \end{cases} \tag{1}$$

A. Chertock (✉) · Ş. N. Özcan
Department of Mathematics, North Carolina State University, 2311 Stinson Drive, 27695 Raleigh, NC, USA
e-mail: chertock@math.ncsu.edu

Ş. N. Özcan
e-mail: snozcan@ncsu.edu

M. Herty
Department of Mathematics, RWTH Aachen University, Templergraben 55, 52056 Aachen, Germany
e-mail: herty@igpm.rwth-aachen.de

C. Klingenberg and M. Westdickenberg (eds.), *Theory, Numerics and Applications of Hyperbolic Problems I*, Springer Proceedings in Mathematics & Statistics 236,
https://doi.org/10.1007/978-3-319-91545-6_28

which can be rewritten in the vector form as

$$\mathbf{U}_t + \boldsymbol{F}(\mathbf{U})_x = \boldsymbol{S}(\mathbf{U}), \tag{2}$$

where

$$\mathbf{U} := \begin{pmatrix} \rho \\ q \end{pmatrix}, \qquad \boldsymbol{F}(\mathbf{U}) := \begin{pmatrix} f_1(\rho, q) \\ f_2(\rho, q) \end{pmatrix}, \qquad \boldsymbol{S}(\mathbf{U}) := \begin{pmatrix} 0 \\ -s(\rho, q) \end{pmatrix}, \tag{3}$$

are the vectors of the conservative variables, flux, and source terms, respectively, and $x \in \mathbb{R}$ and $t \in \mathbb{R}^+$ are the spatial and time variables. Systems of type (1) are called balance laws and appear as mathematical models in many applications, see, e.g., [6, 13, 15, 17, 38]. System (1) is also a common model for gas flow in high-pressure transmission pipelines [3, 35] and traffic flow [2, 12], both will be our primal motivation for designing of a numerical method and validating computational results.

One of the main difficulties one may encounter when numerically solving systems (1) is the loss of smoothness of the solution. Typically, the solutions of these systems possess complicated nonlinear waves such as shocks and rarefaction waves. Capturing such solutions numerically requires the use of high-resolution shock-capturing techniques, see e.g., [37, 39]. In addition to capturing the discontinuities, preserving certain steady states is an essential part of such problems. In many relevant examples, small perturbations of the steady states are also obtained as a solution of balance laws and these perturbations may not be accurately handled on a coarse mesh. Thus, one needs to implement the so-called well-balanced (WB) schemes which are capable of balancing flux and source terms exactly and maintain the small perturbations of the steady states in an accurate and stable way. These methods were first established in [20] and then developed and used widely in many hyperbolic systems, such as shallow water equations [1, 4, 8, 10, 11, 16, 21, 30, 32, 34], Euler equations with gravitation [5, 9, 22, 41–43], etc.

In this paper, we propose a WB Godunov-type finite volume scheme, which conserves the steady-state solutions of (1) exactly. These schemes consist of reconstruction-evolution- projection procedure, in which cell averages of the variables are employed. In particular, we consider a second-order central-upwind (CU) scheme which was first introduced in [27] in the context of the hyperbolic conservation laws and further developed in [24, 25, 28].

The steady states, $\rho_t = q_t = 0$, of (1) satisfy the following time-independent system:

$$\begin{cases} f_1(\rho, q)_x = 0, \\ f_2(\rho, q)_x = -s(\rho, q), \end{cases} \tag{4}$$

as well as $f_1(\rho, q)_t = f_2(\rho, q)_t = s(\rho, q)_t = 0$, which yields

$$f_1(\rho, q) \equiv \text{Const}, \quad f_2(\rho, q) + \int^x s(\rho, q) d\xi \equiv \text{Const}, \quad \forall x, t. \tag{5}$$

Our method is based on incorporating the source term into the flux in the second equation of the system (1) and introducing a new reconstruction-evolution process to guarantee that all steady states of (1) are captured exactly. Following [9, 10], we introduce new equilibrium variables, which are preserved during the reconstruction and propagate in time according to a modified evolution step.

The rest of the paper is organized as follows. In Sect. 2, we outline a second-order CU scheme and its WB modification with the reconstruction of the equilibrium variables in place of the conservative ones and revised numerical fluxes. In Sect. 3, we apply the WB scheme to the examples of the gas transmission systems, particularly the isothermal Euler equations with source term depends on friction or bottom profile. We also apply the method to the Aw–Rascle–Zhang traffic flow model with relaxation terms [2].

2 Numerical Method

In this section, we describe a second-order semi-discrete CU scheme originally introduced in [27] and show that it does not balance the source and flux terms exactly at the discrete level. We, then, present a modification for the reconstruction procedure as well as the numerical flux used in the CU scheme to guarantee the exact preservation of the steady states.

2.1 Second-Order Central-Upwind Scheme

We discretize the computational domain Ω into finite volume cells, $C_j = [x_{j-\frac{1}{2}}, x_{j+\frac{1}{2}}]$ of size Δx centered at $x_j = (j - 1/2)\Delta x$, $j = 1, \ldots, N$, where N is the total number of grid cells in Ω.

We assume that the approximated cell averages of the computed solution at fixed time level t,

$$\bar{\mathbf{U}}_j(t) := \frac{1}{\Delta x}\int\limits_{C_j} \mathbf{U}(x,t)dx, \tag{6}$$

are known.

Considering the system (1), we write the semi-discrete CU scheme as described in, e.g., [23, 26, 36]:

$$\frac{d}{dt}\bar{\mathbf{U}}_j = -\frac{\mathscr{F}_{j+\frac{1}{2}} - \mathscr{F}_{j-\frac{1}{2}}}{\Delta x} + \bar{\mathbf{S}}_j, \tag{7}$$

where, $\mathscr{F}_{j+\frac{1}{2}}$ are the numerical fluxes:

$$\begin{aligned}\mathscr{F}_{j+\frac{1}{2}} &= \frac{a^+_{j+\frac{1}{2}}\boldsymbol{F}(\mathbf{U}^{\mathrm{E}}_j) - a^-_{j+\frac{1}{2}}\boldsymbol{F}(\mathbf{U}^{\mathrm{W}}_{j+1})}{a^+_{j+\frac{1}{2}} - a^-_{j+\frac{1}{2}}} + \alpha_{j+\frac{1}{2}}(\mathbf{U}^{\mathrm{W}}_{j+1} - \mathbf{U}^{\mathrm{E}}_j),\\ \alpha_{j+\frac{1}{2}} &:= \frac{a^+_{j+\frac{1}{2}}a^-_{j+\frac{1}{2}}}{a^+_{j+\frac{1}{2}} - a^-_{j+\frac{1}{2}}},\end{aligned} \tag{8}$$

and $\overline{\boldsymbol{S}}_j$ is the vector of the cell averages of the source term:

$$\overline{\boldsymbol{S}}_j = (0, -s(\overline{\rho}_j, \overline{q}_j))^T. \tag{9}$$

In (8), $\mathbf{U}^{\mathrm{E}}_j$ and $\mathbf{U}^{\mathrm{W}}_{j+1}$ are the left and right point values of the solution at the cell interfaces $x = x_{j+\frac{1}{2}}$ computed by using the piecewise linear reconstruction:

$$\widetilde{\mathbf{U}}(x) = \overline{\mathbf{U}}_j + (\mathbf{U}_x)_j(x - x_j), \quad x \in C_j, \tag{10}$$

that is,

$$\begin{aligned}\mathbf{U}^{\mathrm{E}}_j &:= \widetilde{\mathbf{U}}(x_{j+\frac{1}{2}} - 0) = \overline{\mathbf{U}}_j + \frac{\Delta x}{2}(\mathbf{U}_x)_j,\\ \mathbf{U}^{\mathrm{W}}_{j+1} &:= \widetilde{\mathbf{U}}(x_{j+\frac{1}{2}} + 0) = \overline{\mathbf{U}}_{j+1} - \frac{\Delta x}{2}(\mathbf{U}_x)_{j+1}.\end{aligned} \tag{11}$$

The reconstruction (10) yields a second-order accurate scheme-provided slopes $(\mathbf{U}_x)_j$ give at least first-order approximations to the derivative $\mathbf{U}_x(x_j, t)$. To avoid oscillations, the slopes $(\mathbf{U}_x)_j$ are to be computed using a nonlinear limiter applied to the cell averages $\overline{\mathbf{U}}_j$. In our experiments reported below, we have used a generalized minmod limiter (see e.g., [29, 33, 40]):

$$(\mathbf{U}_x)_j = \mathrm{minmod}\left(\theta\,\frac{\overline{\mathbf{U}}_{j+1} - \overline{\mathbf{U}}_j}{\Delta x}, \frac{\overline{\mathbf{U}}_{j+1} - \overline{\mathbf{U}}_{j-1}}{2\Delta x}, \theta\,\frac{\overline{\mathbf{U}}_j - \overline{\mathbf{U}}_{j-1}}{\Delta x}\right), \quad \theta \in [1, 2], \tag{12}$$

where

$$\mathrm{minmod}(z_1, z_2, \ldots) := \begin{cases}\min(z_1, z_2, \ldots), & \text{if } z_i > 0 \ \forall i,\\ \max(z_1, z_2, \ldots), & \text{if } z_i < 0 \ \forall i,\\ 0, & \text{otherwise,}\end{cases} \tag{13}$$

and the parameter θ is used to control the amount of the numerical dissipation—the larger θ results in less dissipative, but more oscillatory scheme.

The one-sided local speeds of propagation, $a^{\pm}_{j+\frac{1}{2}}$, in (8) are obtained from the largest and smallest eigenvalues $\lambda(\boldsymbol{U})$ of the Jacobian matrix $\partial\boldsymbol{F}(\mathbf{U})/\partial\mathbf{U}$:

$$a^+_{j+\frac{1}{2}} = \max\left\{\lambda(\mathbf{U}^{\mathrm{E}}_j), \lambda(\mathbf{U}^{\mathrm{W}}_{j+1}), 0\right\}, \quad a^-_{j+\frac{1}{2}} = \min\left\{\lambda(\mathbf{U}^{\mathrm{E}}_j), \lambda(\mathbf{U}^{\mathrm{W}}_{j+1}), 0\right\}. \tag{14}$$

Finally, the semi-discrete ODE system, (7) should be integrated in time by an appropriate accurate and stable ODE solver for which the CFL condition satisfies (see e.g., [26])

$$\Delta t \le \kappa \frac{\Delta x}{\max\limits_j |a^{\pm}_{j+\frac{1}{2}}|}, \quad \kappa \le \frac{1}{2}. \tag{15}$$

It is instructive to note that the described scheme does not necessarily preserve the steady-state solutions (5). To cite an example, we consider the case where $f_1(\rho, q) = q$ and, therefore, $q = \text{Const}$ and $\rho = \rho(x)$ satisfies the steady state (5). Implementing the CU scheme (7)–(14) for, say, the first component of the solution will result in the following semi-discrete approximation:

$$\begin{aligned}\frac{d\,\overline{\rho}_j}{dt} = -\frac{1}{\Delta x}\Bigg[&\frac{a^+_{j+\frac{1}{2}} q^{\mathrm{E}}_j - a^-_{j+\frac{1}{2}} q^{\mathrm{W}}_{j+1}}{a^+_{j+\frac{1}{2}} - a^-_{j+\frac{1}{2}}} + \alpha_{j+\frac{1}{2}}(\rho^{\mathrm{W}}_{j+1} - \rho^{\mathrm{E}}_j)\\ &- \frac{a^+_{j-\frac{1}{2}} q^{\mathrm{E}}_{j-1} - a^-_{j-\frac{1}{2}} q^{\mathrm{W}}_j}{a^+_{j-\frac{1}{2}} - a^-_{j-\frac{1}{2}}} + \alpha_{j-\frac{1}{2}}(\rho^{\mathrm{W}}_j - \rho^{\mathrm{E}}_{j-1})\Bigg].\end{aligned}$$

The last equation reduces to

$$\frac{d\,\overline{\rho}_j}{dt} = -\frac{\alpha_{j+\frac{1}{2}}(\rho^{\mathrm{W}}_{j+1} - \rho^{\mathrm{E}}_j) - \alpha_{j-\frac{1}{2}}(\rho^{\mathrm{W}}_j - \rho^{\mathrm{E}}_{j-1})}{\Delta x}, \tag{16}$$

since $q^{\mathrm{E}}_j = q^{\mathrm{W}}_{j+1} = q^{\mathrm{E}}_{j-1} = q^{\mathrm{W}}_j = \text{Const}$. However, in general, the piecewise linear approximation, (10), forms discontinuities at the cell interfaces, so that the point values ρ^{W}_{j+1} and ρ^{E}_j (ρ^{W}_j and ρ^{E}_{j-1}) are not necessarily equal. Thus, right-hand side of the ODE (16) does not vanish and the scheme fails to preserve the steady state.

2.2 Well-Balanced Modification

In this section, we present a WB modification of the CU scheme described in the previous section. To this end, we first define new variables

$$K := f_1(\rho, q), \quad \text{and} \quad L := f_2(\rho, q) + R, \quad R := \int^x s(\xi, \rho, q)d\xi, \tag{17}$$

and rewrite the system as

$$\begin{cases} \rho_t + K_x = 0, \\ q_t + L_x = 0, \end{cases} \tag{18}$$

which can be put into the vector form (2) with the different flux and zero source term: where $\mathbf{U} = (\rho, q)^T$, $\boldsymbol{F}(\mathbf{U}) = (K, L)^T$ and $\boldsymbol{S}(\mathbf{U}) \equiv (0, 0)^T$. Obviously, the steady state of (18) will be in the following form:

$$K \equiv \text{Const}, \qquad L \equiv \text{Const}. \tag{19}$$

2.2.1 Reconstruction

We start by describing a special reconstruction procedure, which is implemented to obtain the point values, $\mathbf{U}_j^{\mathrm{E}}$ and $\mathbf{U}_{j+1}^{\mathrm{W}}$, used in (8), and is based on reconstructing equilibrium variables, K and L, instead of conservative ones, ρ and q. To this end, we first compute the values K_j and L_j from the cell averages, $\overline{\rho}_j$ and $\overline{q}_j$, i.e.,

$$K_j = f_1(\overline{\rho}_j, \overline{q}_j), \qquad L_j = f_2(\overline{\rho}_j, \overline{q}_j) + R_j, \tag{20}$$

where the values of R_j are evaluated by applying the midpoint quadrature rule to the integral in (17) and using the following recursive relation:

$$R_j = \frac{1}{2}(R_{j-\frac{1}{2}} + R_{j+\frac{1}{2}}), \qquad R_{j+\frac{1}{2}} = R(x_{j+\frac{1}{2}}) = R_{j-\frac{1}{2}} + \Delta x\, s(x_j, \overline{\rho}_j, \overline{q}_j), \tag{21}$$

starting from $R_{1/2} \equiv 0$.

The point values of K and L at the cell interfaces $x = x_{j\pm\frac{1}{2}}$ are then obtained from (10)–(13):

$$\begin{aligned} K_j^{\mathrm{E}} &= K_j + \frac{\Delta x}{2}(K_x)_j, \quad L_j^{\mathrm{E}} = L_j + \frac{\Delta x}{2}(L_x)_j, \\ K_j^{\mathrm{W}} &= K_j - \frac{\Delta x}{2}(K_x)_j, \quad L_j^{\mathrm{W}} = L_j - \frac{\Delta x}{2}(L_x)_j. \end{aligned} \tag{22}$$

Finally, equipped with the values of $K_j^{\mathrm{E,W}}$, $L_j^{\mathrm{E,W}}$, and $R_{j\pm\frac{1}{2}}$, we compute the corresponding point values of ρ and q by solving the following four nonlinear equations in terms of ρ_j^{E}, ρ_j^{W}, q_j^{E}, and q_j^{W}, respectively:

$$\begin{aligned} K_j^{\mathrm{E}} &= f_1(\rho_j^{\mathrm{E}}, q_j^{\mathrm{E}}), \qquad L_j^{\mathrm{E}} = f_2(\rho_j^{\mathrm{E}}, q_j^{\mathrm{E}}) + R_{j+\frac{1}{2}}, \\ K_j^{\mathrm{W}} &= f_1(\rho_j^{\mathrm{W}}, q_j^{\mathrm{W}}), \quad L_j^{\mathrm{W}} = f_2(\rho_j^{\mathrm{W}}, q_j^{\mathrm{W}}) + R_{j-\frac{1}{2}}. \end{aligned}$$

Clearly, the procedure would significantly simplify when one of the conservative variables is also an equilibrium one, say, $K = f_1(\rho, q) = q$. In such case, the point values $q_j^{\mathrm{E,W}}$ can be obtained directly from (10)–(13) and thus only two nonlinear equations should be solved to obtain $\rho_j^{\mathrm{E,W}}$ for each j. In all of our examples presented below, the set of nonlinear equations (22) was solved analytically.

2.2.2 Evolution

We then evolve the cell averages, $\bar{\mathbf{U}}_j = (\bar{\rho}_j, \bar{q}_j)^T$, in time by using the following system of ODEs:

$$\frac{d}{dt}\bar{\mathbf{U}}_j = -\frac{\boldsymbol{\mathcal{F}}_{j+\frac{1}{2}} - \boldsymbol{\mathcal{F}}_{j-\frac{1}{2}}}{\Delta x}, \tag{23}$$

where $\boldsymbol{\mathcal{F}}_{j\pm\frac{1}{2}}$ are the numerical fluxes whose two components are given as follows:

$$\begin{aligned}
\mathcal{F}^{(1)}_{j+\frac{1}{2}} &= \frac{a^+_{j+\frac{1}{2}} K^{\mathrm{E}}_j - a^-_{j+\frac{1}{2}} K^{\mathrm{W}}_{j+1}}{a^+_{j+\frac{1}{2}} - a^-_{j+\frac{1}{2}}} \\
&\quad + \alpha_{j+\frac{1}{2}} (\rho^{\mathrm{W}}_{j+1} - \rho^{\mathrm{E}}_j)\, \mathscr{H}\left(\frac{|K_{j+1} - K_j|}{\Delta x} \cdot \frac{|\Omega|}{\max_j\{K_j, K_{j+1}\}}\right), \\
\mathcal{F}^{(2)}_{j+\frac{1}{2}} &= \frac{a^+_{j+\frac{1}{2}} L^{\mathrm{E}}_j - a^-_{j+\frac{1}{2}} L^{\mathrm{W}}_{j+1}}{a^+_{j+\frac{1}{2}} - a^-_{j+\frac{1}{2}}} \\
&\quad + \alpha_{j+\frac{1}{2}} (q^{\mathrm{W}}_{j+1} - q^{\mathrm{E}}_j)\, \mathscr{H}\left(\frac{|L_{j+1} - L_j|}{\Delta x} \cdot \frac{|\Omega|}{\max_j\{L_j, L_{j+1}\}}\right),
\end{aligned} \tag{24}$$

and $\alpha_{j+\frac{1}{2}}$ is defined in (8). The second components in the numerical flux functions (24) are modified (compared to (8)) to accommodate to preserve the steady states. Namely, a smooth function $\mathscr{H}$, satisfying

$$\mathscr{H}(\phi) = \frac{(C\phi)^m}{1 + (C\phi)^m}, \quad \mathscr{H}(0) = 0, \tag{25}$$

is introduced for some constants $C > 0$ and $m > 0$. When the solution is a steady state, e.g., both $K^{\mathrm{E}}_j = K^{\mathrm{W}}_{j+1} = K_j \equiv \text{Const}$ and $L^{\mathrm{E}}_j = L^{\mathrm{W}}_{j+1} = L_j \equiv \text{Const}$, $\mathscr{H}$ vanishes, so is each component of the numerical flux in (24). Otherwise, $\mathscr{H}$ is very close to 1 and then the scheme reduces to the classical semi-discrete central-upwind scheme (8). The normalization factors, $\frac{|\Omega|}{\max_j\{K_j, K_{j+1}\}}$ and $\frac{|\Omega|}{\max_j\{L_j, L_{j+1}\}}$, where $|\Omega|$ is the size of the computational domain, are introduced in order to make the function $\mathscr{H}$ nondimensional and independent of the choice of C and m. We summarize this observation in the following theorem.

Theorem 1 *The semi-discrete CU scheme, (23)–(25), with the reconstruction described in Sect. 2.2.1 gives an absolute balance between the source and flux terms and thus preserves the steady state, (5), exactly, i.e., the scheme is WB.*

Proof Let us start with assuming that at a certain time level t the solution reaches its steady state and

$$K_j^{\mathrm{E}} = K_{j+1}^{\mathrm{W}} = K_j \equiv K^* \quad \text{and} \quad L_j^{\mathrm{E}} = L_{j+1}^{\mathrm{W}} = L_j \equiv L^*, \qquad \forall j, \tag{26}$$

where K^* and L^* are constants. We show that $\bar{\mathbf{U}}_j = (\bar{\rho}_j, \bar{q}_j)^T$ remains constant in time, which means the right-hand side of the ODE system (23) diminishes with given conditions (26). Indeed, identities in (26) imply $\mathscr{H} = 0$, which in turns results in $\mathscr{F}^{(1)}_{j+\frac{1}{2}} = K^*$ and $\mathscr{F}^{(2)}_{j+\frac{1}{2}} = L^*$. Therefore, both $\mathscr{F}^{(1)}_{j+\frac{1}{2}} - \mathscr{F}^{(1)}_{j-\frac{1}{2}} = 0$ and $\mathscr{F}^{(2)}_{j+\frac{1}{2}} - \mathscr{F}^{(2)}_{j-\frac{1}{2}} = 0$ and thus from (23) we obtain $\dfrac{d\,\bar{\mathbf{U}}_j}{dt} = 0, \ \forall j.$

□

3 Computational Results

In this section, we test the performance of the developed WB method and show that it preserves steady-state solutions exactly for several 2×2 systems. In particular, the system of isothermal Euler equations of gas dynamics with friction and with the bottom profile and the model for traffic flow with relaxation are studied.

In all of the experiments reported below, we implemented the second-order WB CU scheme (23)–(25) and compared the obtained results with those computed by the non well-balanced (NWB) CU scheme (7)–(9). The scheme parameters were taken as $\theta = 1.3$ in Examples 1, 2 and $\theta = 1$ in Example 3; $C = 200$ in Examples 1, 3 and $C = 400$ in Example 2 and $m = 1$ in (25) in all of the examples. For the time evolution, we used the third-order strong stability preserving Runge–Kutta method (see, e.g., [18, 19]) to solve the semi-discrete ODE system (23) with the CFL constant in (15) taken as $\kappa = 0.4$ in Examples 1, 3 and $\kappa = 0.1$ in Example 2.

Example 1 – Gas dynamics with pipe-wall friction. In this example, we solve the isothermal Euler equations of gas dynamics with pipe-wall friction, which is used for the simulation of high-pressure gas transmission systems [7, 35]. The model is governed by the following system of hyperbolic balance laws:

$$\begin{cases} \rho_t + q_x = 0, \\ q_t + \left(c^2\rho + \dfrac{q^2}{\rho}\right)_x = -\mu\dfrac{q}{\rho}|q|, \end{cases} \tag{27}$$

where $\rho(x,t)$ is the density of the fluid with the velocity $u(x,t)$, $q(x,t)$ is the momentum, $\mu > 0$ is the friction coefficient (divided by the pipe cross section) and $c > 0$ is the speed of sound.

We first check the WB property of the developed scheme by considering (27) with $c = \mu = 1$ and subject to the following initial data (given in terms of equilibrium variables):

$$K(x,0) = q(x,0) = K^* = 0.15 \quad \text{and} \quad L(x,0) = L^* = 0.4, \tag{28}$$

in a single pipe $x \in [0,1]$. Here,

$$K(x,t) = q(x,t) \quad \text{and} \quad L(x,t) = \left(c^2\rho + \frac{q^2}{\rho}\right)(x,t) + R(x,t), \tag{29}$$

are the steady states and $R(x,t) = \int^x \mu \dfrac{q(\xi,t)}{\rho(\xi,t)}|q(\xi,t)|d\xi$.

To run the computations, we divide the interval $\Omega = [0,1]$ into N uniform grid cells and apply the WB second-order CU scheme (23)–(25) to the system (27) with zero-order extrapolations for both K and L at the boundaries of the domain. We compute the solution until the final time $T = 1$ with $N = 100$, 200, 400 and 800 and report L^1-errors, measured as $\|K(\cdot,T) - K^*\|_1$ and $\|L(\cdot,T) - L^*\|_1$, in Table 1 (left). As one can see, on all of these grids, the initial data are preserved within the machine accuracy. For comparison, we run the same computations using the NWB CU scheme (7)–(9), in which case the initial equilibria are preserved within the accuracy of the scheme only, as can be seen in Table 1 (right).

Next, we solve the system (27) with the perturbed initial data as follows:

$$K(x,0) = K^* + \eta e^{-100(x-0.5)^2} = 0.5 + \eta e^{-100(x-0.5)^2}, \quad L(x,0) = L^* = 0.4, \tag{30}$$

with the perturbation constant $\eta > 0$. In Fig. 1, we plot the obtained momentum perturbations computed using both WB and NWB schemes with two different perturbation constants, $\eta = 10^{-3}$ and $\eta = 10^{-6}$ at time $T = 0.2$ on $N = 100$ uniform grid cells. We also calculate a solution using the NWB method on finer grids, i.e., $N = 1600$ for $\eta = 10^{-3}$ and $N = 3200$ for $\eta = 10^{-6}$. We observe that for the larger value of the constant $\eta = 10^{-3}$, both the WB and NWB schemes can capture the perturbation even on a coarse mesh. However, when the perturbation is relatively small, $\eta = 10^{-6}$, the WB scheme still can resolve the perturbation on a coarse grid

Table 1 Example 1: L^1-errors of the results from the WB (left) and NWB (right) computations at time $T = 1$

N	q	K
100	1.94E-18	7.77E-18
200	9.71E-19	9.71E-18
400	1.66E-18	9.57E-18
800	2.18E-18	1.18E-17

N	q	Rate	K	Rate
100	1.29E-06	–	8.81E-07	–
200	3.30E-07	1.9668	2.25E-07	1.9692
400	8.34E-08	1.9843	5.69E-08	1.9834
800	2.09E-08	1.9965	1.43E-08	1.9924

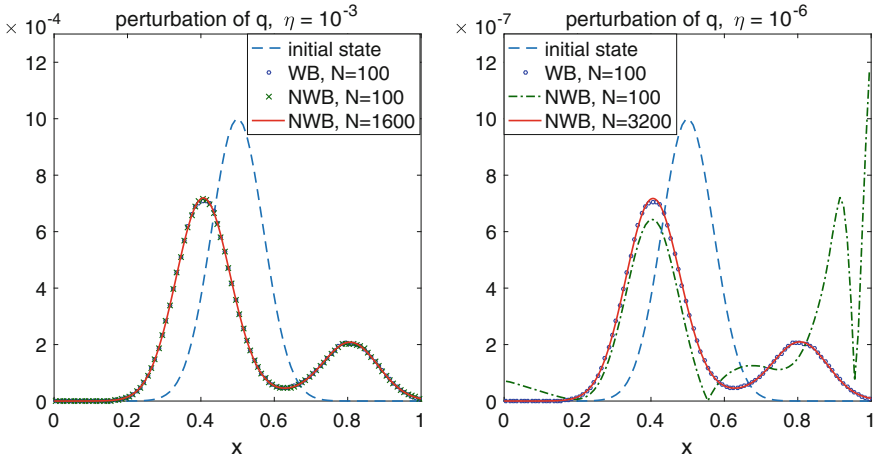

Fig. 1 Example 1: Momentum perturbation computed by the WB and NWB schemes at time $T = 0.2$ for $\eta = 10^{-3}$ (left) and $\eta = 10^{-6}$ (right)

($N = 100$), while the NWB method is not capable of catching it unless it is employed on a very fine mesh, say $N = 3200$.

Example 2 – Gas dynamics with the bottom profile. In the second example, we consider the 2×2 system of gas dynamics with bottom profile where the governing equations are given by

$$\begin{cases} \rho_t + q_x = 0, \\ q_t + \left(c^2\rho + \dfrac{q^2}{\rho}\right)_x = -g\rho h_x(x), \end{cases} \tag{31}$$

with $h(x)$ being the bottom profile. This case is relevant to the practical applications when gas pipes are not horizontal. In particular, the gravitational force needs to be considered in mountainous regions with high-pressure gas transmission.

Here, we consider the system (31) with $c = 1$, $g = 9.81$ and an exponential function

$$h(x) = e^{-(x-0.5)^2}. \tag{32}$$

We solve the system on the computational domain $x \in [0, 1]$ and subject to the following initial data (again given in terms of equilibrium variables):

$$K(x, 0) = q(x, 0) = K^* = 1 \quad \text{and} \quad L(x, 0) = L^* = 20, \tag{33}$$

Table 2 Example 2: L^1-errors of the results from the WB (left) and NWB (right) computations at time $T = 1$

N	q	K	N	q	Rate	K	Rate
100	3.19E-16	1.17E-15	100	8.97E-03	–	0.117	–
200	3.90E-16	9.76E-16	200	2.25E-03	1.9951	2.98E-02	1.9731
400	1.99E-16	8.70E-16	400	5.64E-04	1.9961	7.54E-03	1.9826
800	1.41E-16	9.45E-16	800	1.41E-04	2.0000	1.89E-03	1.9972

where

$$K(x,t) = q(x,t) \quad \text{and} \quad L(x,t) = \left(c^2\rho + \frac{q^2}{\rho}\right)(x,t) + R(x,t), \tag{34}$$

and $R = \int^x g\rho(\xi,t)h_x(\xi)d\xi$. Since (33) is a steady-state solution of (31), we adopt it to illustrate that the CU scheme (23)–(25) is WB.

Similarly to the first example, we obtain the solutions of the system (31) by implementing both the WB and NWB CU schemes on a uniform grid with $N =$ 100, 200, 400 and 800 cells. Table 2 indicates the L^1-errors as estimated in the previous example in measuring the equilibrium states K and L computed by both the WB (left) and NWB (right) schemes. One can clearly see that while the WB scheme gives errors within machine accuracy, the NWB method requires very fine grid, to preserve steady- state solution.

We, then, introduce an initial perturbation on momentum as follows:

$$K(x,0) = K^* + \eta e^{-100(x-0.5)^2} = 1 + \eta e^{-100(x-0.5)^2}, \quad L(x,0) = L^* = 20, \tag{35}$$

where $\eta > 0$ is the perturbation constant. We first run the computations with $\eta = 10^{-1}$ and plot the results in Fig. 2 (left) obtained at time $T = 0.25$ by both the WB and NWB methods with $N = 100$ uniform grid cells. In both cases, zero-order extrapolations are implemented at the boundaries of the computational interval $\Omega = [0, 1]$. For comparison, we also plot a solution obtained by the NWB scheme with $N = 1600$. We observe that, while the WB scheme is capable of resolving the perturbation on a coarse mesh, the NWB method requires a finer mesh, e.g., $N = 1600$. In Fig. 2 (right), we illustrate the momentum perturbation at time $T = 0.25$ obtained by both the WB and NWB schemes for a smaller value of the perturbation constant $\eta = 10^{-3}$. We note that our WB scheme can capture smaller perturbations of the steady states on a coarse mesh, $N = 100$, while to obtain corresponding results with the NWB method, one needs to use a very refined mesh, $N = 6400$, which would be costly in most of the cases.

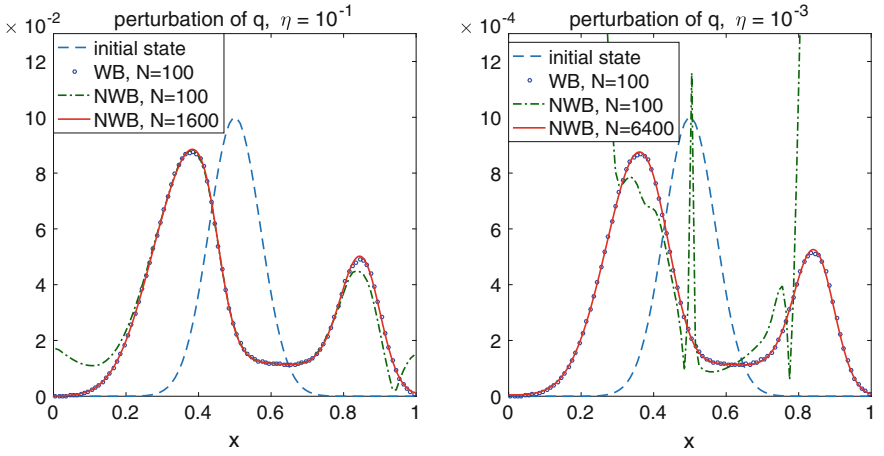

Fig. 2 Example 2: Momentum perturbations computed by the WB and NWB schemes for $\eta = 10^{-1}$ (left) and $\eta = 10^{-3}$ (right) at time $T = 0.25$

Example 3 – Traffic flow with relaxation to equilibrium velocities. In the last example, we study a second-order model for traffic flow, which has been introduced in [2] to model driver-dependent traffic conditions. The model has been investigated since then by many authors and we refer to [14] for a recent comparison and discussion.

The governing equations are written in terms of the density of cars $\rho(x,t)$ and the velocity $u(x,t)$, as well as a driver property $w(x,t)$. The latter can be viewed as distance towards an equilibrium velocity $V_{eq}(\rho)$. For simplicity, we chose as $V_{eq}(\rho) = 1-\rho$, where $\rho = 1$ represents maximum density and introduce a fixed relaxation time $\tau > 0$ for all drivers, in which case the model reads as follows:

$$\begin{cases} \rho_t + (\rho u)_x = 0, \\ (\rho w)_t + (\rho u w)_x = \dfrac{\rho}{\tau}\left((1-\rho) - u\right), \\ w = u + \rho. \end{cases}$$

We substitute $u = w - \rho$, introduce a new variable $q = \rho u = \rho(w-1)$ and rewrite the above system in the conservative form as follows:

$$\begin{cases} \rho_t + (q + \rho(1-\rho))_x = 0, \\ q_t + \left(\dfrac{q^2}{\rho} + q(1-\rho)\right)_x = -\dfrac{1}{\tau} q. \end{cases} \tag{36}$$

We observe that in the limit of small relaxation times ($\tau \to 0$), the second equation in (36) formally ensures $q \to 0$ and $\rho \in [0,1]$, and the model predictions of (36) are

expected to be close to those of the classical Lighthill–Whitham–Richards (LWR) model [31] given by $\rho_t + (\rho(1-\rho))_x = 0$.

Clearly, $q = 0$ is a steady-state solution of the system (36) for any constant ρ. However, for fixed positive τ, the system has steady states deviating from the LWR model. In view of the previous discussion, we introduce the equilibrium variables K and L as

$$K = q + \rho(1-\rho), \quad L = \frac{q^2}{\rho} + q(1-\rho) + R, \tag{37}$$

where $R(x,t) = \int^x \frac{1}{\tau} q(\xi,t)d\xi$. Then, the steady states are K, L =Const.

We consider the system (36) with $\tau = 1$ and set the following initial data given with respect to the equilibrium variables:

$$K(x,0) = K^* = 0.375, \quad L(x,0) = L^* = 0.5, \tag{38}$$

which also satisfy the steady-state solutions of (36).

As before, we first verify that the developed WB CU scheme (23)–(25) is capable of preserving steady states of the system (36) exactly. To this end, we partition the computational domain $\Omega = [0,1]$ into N uniform cells and assign zero-order extrapolations for K and L at the boundaries. We obtain the results at final time $T = 1$ by implementing the WB CU scheme with $N = 100,\ 200,\ 400$, and 800 grid cells. In Table 3 (left), we present the L^1-errors computed as before, for equilibrium variables K and L, that is, $\|K(\cdot,T) - K^*\|_1$ and $\|L(\cdot,T) - L^*\|_1$, and observe that the errors of machine accuracy for the WB scheme. However, we can conclude that NWB scheme can maintain the steady states only within the order of the scheme, as seen in Table 3 (right).

We then investigate the performance of the WB scheme by capturing the perturbations of the steady states. Here, we add a small perturbation to the initial value of the variable q:

$$q^p(x,0) = q(x,0) + \eta e^{-50(x-0.5)^2}, \tag{39}$$

Table 3 Example 3: L^1-errors of the results from the WB (left) and NWB (right) computations at time $T = 1$

N	K	L
100	4.21E-17	1.00E-16
200	5.57E-17	8.74E-17
400	1.48E-15	2.46E-15
800	5.50E-17	1.17E-16

N	K	Rate	L	Rate
100	2.59E-06	–	8.10E-06	–
200	6.47E-07	2.0011	2.02E-06	2.0035
400	1.61E-07	2.0067	5.04E-07	2.0028
800	4.04E-08	1.9946	1.25E-07	2.0114

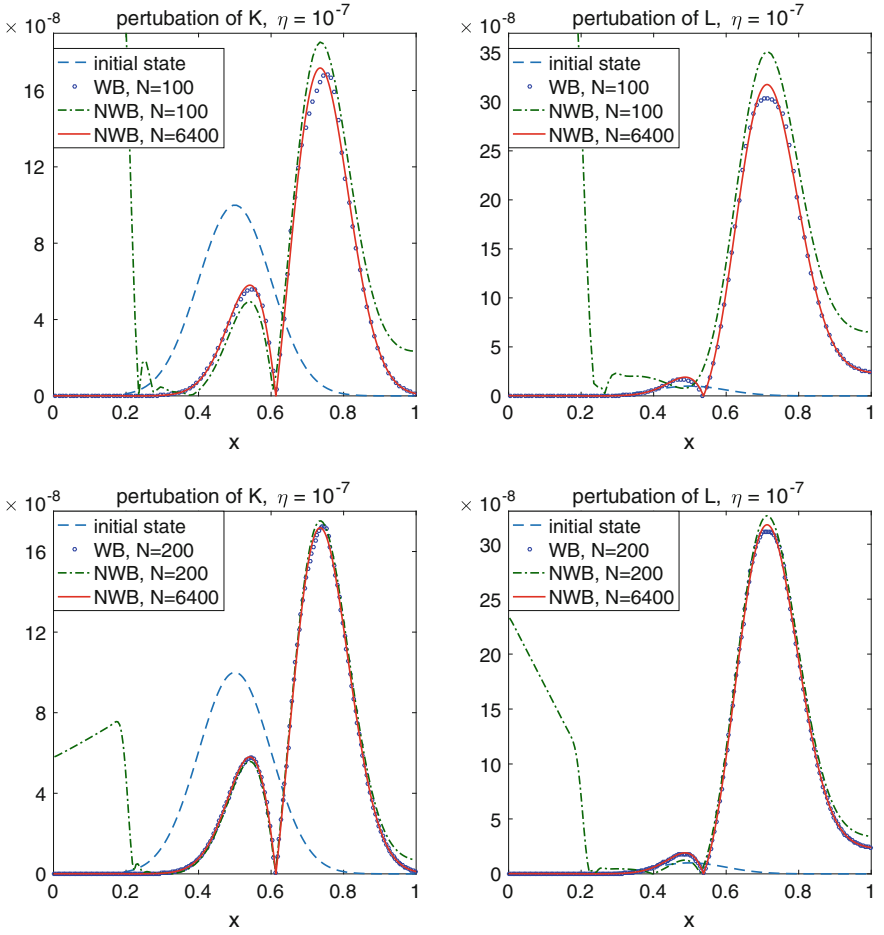

Fig. 3 Example 3: Perturbations on the equilibrium variable K (left column) and L (right column), computed by the WB and NWB schemes at time $T = 0.1$ for $\eta = 10^{-7}$

where $\eta = 10^{-7}$ is taken in this example. In Fig. 3, we plot the perturbations on the equilibrium variables K and L, respectively, obtained by both WB and NWB schemes with $N = 100$ and 200 uniform grid cells at time $T = 0.1$. For observation, we also plot the solutions computed by NWB method on a very fine mesh with $N = 6400$. We conclude that while the WB scheme is capable of capturing the perturbations on a relatively coarse grid, the NWB scheme needs to be implemented on a much finer grid.

4 Conclusion

We have generated a well-balanced second-order central-upwind scheme for 2 × 2 systems of balance laws. This is a first work in a series of well-balanced methods that preserve general steady states of the underlying system. Particularly, we consider gas flow in high-pressure transmission pipelines and traffic model with relaxation. We have presented the results of one-dimensional model, in which, steady states are captured exactly by the proposed well-balanced scheme. As an ongoing study, different physical models including the two-dimensional systems will be examined.

Acknowledgements The work of A. Chertock was supported in part by the NSF Grants DMS-1521051. The work of M. Herty was supported in part by DFG STE2063/1-1 DFG HE5386/13-15, the cluster of excellence DFG EXC128 'Integrative Production Technology for High-Wage Countries' and the BMBF project KinOpt. The work of Ş. N. Özcan was supported in part by the Turkish Ministry of National Education. The authors also acknowledge the support by NSF RNMS Grant DMS-1107444. The authors thank M. Lukáčová for her hospitality at the University of Mainz.

References

1. E. Audusse, F. Bouchut, M.O. Bristeau, R. Klein, B. Perthame, A fast and stable well-balanced scheme with hydrostatic reconstruction for shallow water flows. SIAM J. Sci. Comput. **25**, 2050–2065 (2004)
2. A. Aw, M. Rascle, Resurection of second order models of traffic flow. SIAM J. Appl. Math. **60**, 916–944 (2000)
3. M.K. Banda, M. Herty, A. Klar, Gas flow in pipeline networks. Netw. Heterog. Media **1**(1), 41–56 (2006)
4. A. Bollermann, G. Chen, A. Kurganov, S. Noelle, A well-balanced reconstruction of wet/dry fronts for the shallow water equations. J. Sci. Comput. **56**(2), 267–290 (2013)
5. N. Botta, R. Klein, S. Langenberg, S. Lützenkirchen, Well-balanced finite volume methods for nearly hydrostatic flows. J. Comput. Phys. **196**(2), 539–565 (2004)
6. A. Bressan, S. Canic, M. Garavello, M. Herty, B. Piccoli, Flow on networks: recent results and perspectives. Eur. Math. Soc.-Surv. Math. Sci. **1**(1), 47–111 (2014)
7. J. Brouwer, I. Gasser, M. Herty, Gas pipeline models revisited: model hierarchies, nonisothermal models, and simulations of networks. Multiscale Model. Simul. **9**(2), 601–623 (2011)
8. S. Bryson, Y. Epshteyn, A. Kurganov, G. Petrova, Well-balanced positivity preserving central-upwind scheme on triangular grids for the Saint-Venant system. M2AN. Math. Model. Numer. Anal. **45**(3), 423–446 (2011)
9. A. Chertock, S. Cui, A. Kurganov, Ş.N. Özcan, E. Tadmor, Well-balanced central-upwind schemes for the Euler equations with gravitation (2015) (Submitted)
10. A. Chertock, M. Dudzinski, A. Kurganov, M. Lukáčová-Medvi'ová, Well-balanced schemes for the shallow water equations with Coriolis forces (2014) (Submitted)
11. A. Chinnayya, A.Y. LeRoux, N. Seguin, A well-balanced numerical scheme for the approximation of the shallow water equations with topography: the resonance phenomenon. Int. J. Finite Vol. **1**, 1–33 (2004)
12. Colombo, R.M.: Hyperbolic phase transitions in traffic flow. SIAM J. Appl. Math. **63**(2), 708–721 (electronic) (2002)
13. P.J. Dellar, R. Salmon, Shallow water equations with a complete Coriolis force and topography. Phys. Fluids **17**(106), 601–19 (2005)

14. S. Fan, M. Herty, B. Seibold, Comparative model accuracy of a data-fitted generalized Aw-Rascle-Zhang model. Netw. Heterog. Media **9**(2), 239–268 (2014)
15. L. Forestier-Coste, S. Göttlich, M. Herty, Data-fitted second-order macroscopic production models. SIAM J. Appl. Math. **75**(3), 999–1014 (2015)
16. J.M. Gallardo, C. Parés, M. Castro, On a well-balanced high-order finite volume scheme for shallow water equations with topography and dry areas. J. Comput. Phys. **227**(1), 574–601 (2007)
17. T. Gallouët, J.M. Hérard, N. Seguin, Some approximate Godunov schemes to compute shallow water equations with topography. Comput. Fluids **32**(4), 479–513 (2003)
18. Gottlieb, S., Ketcheson, D.I., Shu, C.W.: Strong stability preserving Runge-Kutta and multistep time discretizations. (World Scientific Publishing Co. Pte. Ltd., Hackensack, NJ, 2011)
19. S. Gottlieb, C.W. Shu, E. Tadmor, Strong stability-preserving high-order time discretization methods. SIAM Rev. **43**, 89–112 (2001)
20. J.M. Greenberg, A.Y. Leroux, A well-balanced scheme for the numerical processing of source terms in hyperbolic equations. SIAM J. Numer. Anal. **33**(1), 1–16 (1996)
21. S. Jin, A steady-state capturing method for hyperbolic systems with geometrical source terms. M2AN. Math. Model. Numer. Anal. **35**(4), 631–645 (2001)
22. R. Käppeli, S. Mishra, Well-balanced schemes for the Euler equations with gravitation. J. Comput. Phys. **259**, 199–219 (2014)
23. A. Kurganov, D. Levy, Central-upwind schemes for the Saint-Venant system. M2AN Math. Model. Numer. Anal. **36**, 397–425 (2002)
24. A. Kurganov, C.T. Lin, On the reduction of numerical dissipation in central-upwind schemes. Commun. Comput. Phys. **2**, 141–163 (2007)
25. A. Kurganov, S. Noelle, G. Petrova, Semi-discrete central-upwind scheme for hyperbolic conservation laws and Hamilton–Jacobi equations. SIAM J. Sci. Comput. **23**, 707–740 (2001)
26. A. Kurganov, G. Petrova, A second-order well-balanced positivity preserving central-upwind scheme for the Saint-Venant system. Commun. Math. Sci. **5**, 133–160 (2007)
27. A. Kurganov, E. Tadmor, New high resolution central schemes for nonlinear conservation laws and convection-diffusion equations. J. Comput. Phys. **160**, 241–282 (2000)
28. A. Kurganov, E. Tadmor, Solution of two-dimensional Riemann problems for gas dynamics without Riemann problem solvers. Numer. Methods Partial Differ. Equ. **18**, 584–608 (2002)
29. B. van Leer, Towards the ultimate conservative difference scheme. V. A second-order sequel to Godunov's method. J. Comput. Phys. **32**, 101–136 (1979)
30. R. LeVeque, Balancing source terms and flux gradients in high-resolution Godunov methods: the quasi-steady wave-propagation algorithm. J. Comput. Phys. **146**(1), 346–365 (1998)
31. Lighthill, M.J., Whitham, G.B.: On kinematic waves. II. A theory of traffic flow on long crowded roads. Proc. Roy. Soc. Lond. Ser. A **229**, 317–345 (1955)
32. M. Lukáčová-Medvid'ová, S. Noelle, M. Kraft, Well-balanced finite volume evolution Galerkin methods for the shallow water equations. J. Comp. Phys. **221**, 122–147 (2007)
33. H. Nessyahu, E. Tadmor, Nonoscillatory central differencing for hyperbolic conservation laws. J. Comput. Phys. **87**(2), 408–463 (1990)
34. S. Noelle, N. Pankratz, G. Puppo, J. Natvig, Well-balanced finite volume schemes of arbitrary order of accuracy for shallow water flows. J. Comput. Phys. **213**(2), 474–499 (2006)
35. A. Osiadacz, *Simulation and Analysis of Gas Networks* (Gulf Publishing Company, Houston, 1989)
36. G. Russo, Central schemes and systems of balance laws, in *Hyperbolic Partial Differential Equations* (Hamburg, 2001), pp. 59–114 (Vieweg, Braunschweig, 2002)
37. G. Russo, High-order shock-capturing schemes for balance laws, in *Numerical Solutions of Partial Differential Equations* (Advanced Mathematics Training Course. CRM Barcelona, 2009), pp. 59–147. (Birkhäuser, Basel, 2009)
38. A. de Saint-Venant, Thèorie du mouvement non-permanent des eaux, avec application aux crues des rivière at à l'introduction des marèes dans leur lit. C.R. Acad. Sci. Paris **73**, 147–154 (1871)

39. C.W. Shu, S. Osher, Efficient implementation of essentially non-oscillatory shock-capturing schemes. J. Comput. Phys. **77**, 439–471 (1988)
40. P. Sweby, High resolution schemes using flux limiters for hyperbolic conservation laws. SIAM J. Numer. Anal. **21**(5), 995–1011 (1984)
41. C.T. Tian, K. Xu, K.L. Chan, L.C. Deng, A three-dimensional multidimensional gas-kinetic scheme for the Navier–Stokes equations under gravitational fields. J. Comput. Phys. **226**(2), 2003–2027 (2007)
42. Y. Xing, C.W. Shu, High order well-balanced WENO scheme for the gas dynamics equations under gravitational fields. J. Sci. Comput. **54**, 645–662 (2013)
43. K. Xu, J. Luo, S. Chen, A well-balanced kinetic scheme for gas dynamic equations under gravitational field. Adv. Appl. Math. Mech. **2**, 200–210 (2010)